Tokyo Climate Center, Japan Meteorological Agency

TCC News

No. 45 Summer 2016

Contents	Page

Incorporation of ENSO Forecast Probabilities into the TCC El Niño Outlook

ENSO forecast probabilities were incorporated into the TCC El Niño Outlook in August 2016.

Forecast probabilities for the onset, persistence and end of ENSO events (El Niño, La Niña and ENSO-neutral periods) were incorporated into the TCC El Niño Outlook in August 2016 for added clarity.

Specifically, information on ENSO event outlooks contained in the lead part and the main body now include probability values regarding ENSO event onset and other considerations. By way of example, the second lead part of the El Niño Outlook in July (before the update) was as follows:

- La Niña conditions are less likely to develop during boreal summer than in the previous month's prediction; La Niña onset is more likely to occur in boreal autumn.

With the new forecast probability information, the lead would be:

- The likelihood of La Niña conditions developing during boreal summer is **40%**, which is lower than in the previous month's prediction.
- Despite a **40%** likelihood that ENSO-neutral conditions will persist until boreal autumn, it is more likely that a La Niña event will begin to develop in autumn (**60%**).

Figure 2 on the "Figures and Tables" page of the outlook shows probability values from two months before the current month to four months after. An example is shown in Figure 1, which suggests that the probability of La Niña onset will become gradually higher during boreal summer and autumn.

Using probability values in the ENSO outlook supports expression of the likelihood of the onset, persistence and

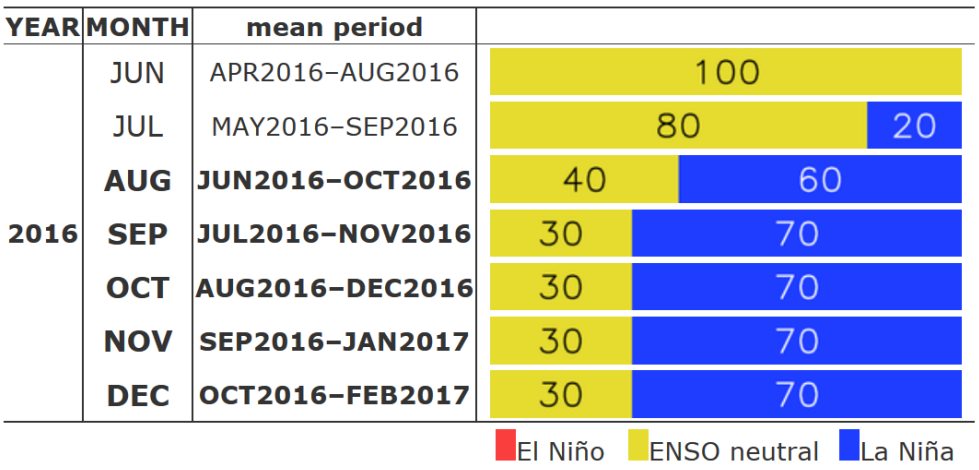

Figure 1 ENSO forecast probabilities based on JMA/MRI-CGCM2 (Fig. 2 in the El Niño Outlook)
Red, yellow and blue bars indicate probabilities that the five-month running mean of the NINO.3 SST deviation from the sliding 30-year mean will be +0.5°C or above (El Niño), between +0.4 and -0.4°C (ENSO-neutral) and -0.5°C or below (La Niña), respectively. Regular text indicates past months, and bold text indicates current and future months.

end of ENSO events with greater precision than simple expressions such as, "It is likely that…" Users are also provided with information on probability changes or tendencies compared to the previous month's outlook.

These probabilities are based on output from the JMA's ENSO prediction model (JMA/MRI-CGCM2), which is also used for three-month prediction and warm-/cold-season prediction. The model is operated as a 51-member ensemble prediction system, and probabilities are essentially calculated as ratios of variables used to predict each event (El Niño, La Niña or ENSO-neutral conditions) before being calibrated using data from the 30-year (1981 – 2010) re-forecast experiment.

The accuracy of ENSO forecast probability data from this procedure is evaluated using re-forecast experiment results. Table 1 shows the performance of the ENSO probprobability forecast for four months ahead. The hit rate for El Niño prediction (i.e., [No. of cases in which El Niño was predicted and occurred (70)] / [Total number of El Niño predictions (104)]) is 67%, and the miss rate (i.e., [No. of cases in which El Niño was not predicted but occurred (27)] / [Total number of El Niño events (97)]) is 28%. For La Niña, the hit rate is 70% (68 / 97) and the miss rate is 26% (24 / 92). Thus, it is considered that when a probability of 50% or higher is predicted, the use of phrases such as, "It is likely that El Niño conditions will develop" is appropriate.

(Ichiro Ishikawa, Climate Prediction Division)

	El Niño	not El Niño	Total
Predict El Niño (Prob≥50%)	70	34	104
Predict not El Niño (Prob<50%)	27	229	256
Total	97	263	360

	La Niña	not La Niña	Total
Predict La Niña (Prob≥50%)	68	29	97
Predict not La Niña (Prob<50%)	24	239	263
Total	92	268	360

Table 1 Contingency tables for ENSO probability forecasts based on 30-year re-forecast experiment data

The top panel shows El Niño probability for four months ahead, and the bottom panel shows La Niña probability. The rows correspond to cases in which the model predicts high probability (≥ 50%), low probability (< 50%) and the total of both. The columns correspond to whether El Niño/La Niña events actually occurred. The figures indicate numbers of cases corresponding to each row and column. The total number of cases is 360 (30 years x 12 months).

Summary of the 2014–16 El Niño event

The El Niño conditions observed from boreal summer 2014 to spring 2016 were the first since 2009–10. During this event, the maximum monthly mean sea surface temperature (SST) deviation in the NINO.3 region (5°S–5°N, 150°W–90°W) was +3.0°C, which was the third highest after the El Niño events of 1997–98 and 1982–83.

1. Outline of the 2014-16 El Niño event

The Japan Meteorological Agency (JMA) monitors sea surface temperature (SST) in the NINO.3 region (5°S–5°N, 150°W–90°W), where interannual variability is the largest in the equatorial Pacific, to identify El Niño/La Niña events (http://ds.data.jma.go.jp/tcc/tcc/products/elnino/index.html). JMA defines El Niño (La Niña) events as periods during which the five-month running mean of NINO.3 SST deviation from the latest 30-year average is +0.5 (–0.5)°C or higher (lower) for at least six consecutive months. Based on this definition, the 2014–16 El Niño event started to develop in boreal summer 2014 (Figure 2). However, the five-month running mean of NINO.3 SST deviation remained slightly above the El Niño threshold of +0.5°C until boreal winter 2014/2015 (December 2014 – February 2015). The event began to strengthen in boreal spring 2015, and the NINO.3 SST deviation reached its peak value of +3.0°C in December 2015. The event then decayed rapidly and terminated in boreal spring 2016, having lasted eight seasons (since boreal summer 2014), which is the longest among the 15 El Niño events that have occurred since 1949.

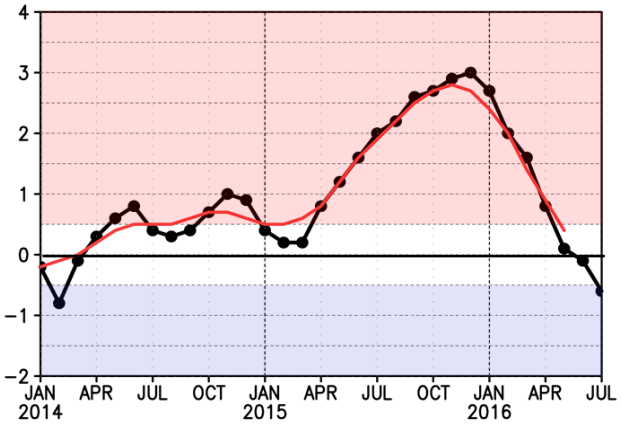

Figure 2 Time series of NINO.3 SST deviation from the latest 30-year average (°C).

Black (red) line indicates monthly mean (five-month running mean).

This event was the strongest for 18 years since that of 1997–98. The monthly mean NINO.3 SST of +3.0°C above the latest 30-year average recorded in December 2015 was the third highest among the 15 occurring since 1949, behind those of 1997–98 and 1982–83 (+3.6 and +3.3°C, respectively; Figure 3).

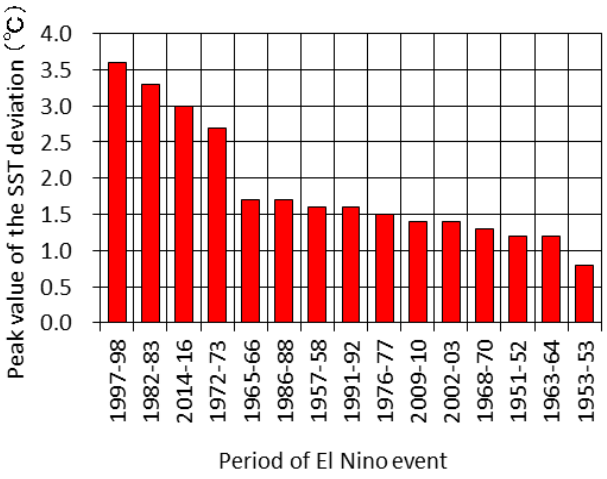

Figure 3 Peak values of NINO.3 SST deviation during each El Niño event since 1949 (°C).
The deviation is a departure from the latest 30-year average in each event.

2. Development of the 2014–16 El Niño event

Figure 4 shows shows time-longitude representations of anomalies in zonal wind stress, SSTs and vertically averaged temperature over the top 300-m layer along the equatorial Pacific. In 2014, two strong westerly wind events (WWEs) occurred over the western equatorial Pacific during the period from January to March. In response, warmer-than-normal subsurface water propagated eastward in the equatorial Pacific, resulting in increased SST anomalies in the eastern equatorial Pacific around May – June 2014. However, further SST increases were subsequently suppressed due to easterly wind anomalies in the central part of the equatorial Pacific in association with the Madden-Julian Oscillation (MJO) in early summer. In February and March 2015, two strong WWEs in the western part of the equatorial Pacific excited warmer-than-normal subsurface water in the central part. As a result, SSTs in the eastern part began to increase in boreal spring 2015. Although these processes were also seen in the first half of 2014, the El Niño event developed due to subsequent significant atmosphere-ocean interaction throughout 2015. In early 2015, colder-than-normal subsurface water that had built up during the El Niño event migrated to the eastern part of the equatorial Pacific, leading to a rapid decrease in SST anomalies there. The 2014–16 El Niño event ended in boreal spring 2016.

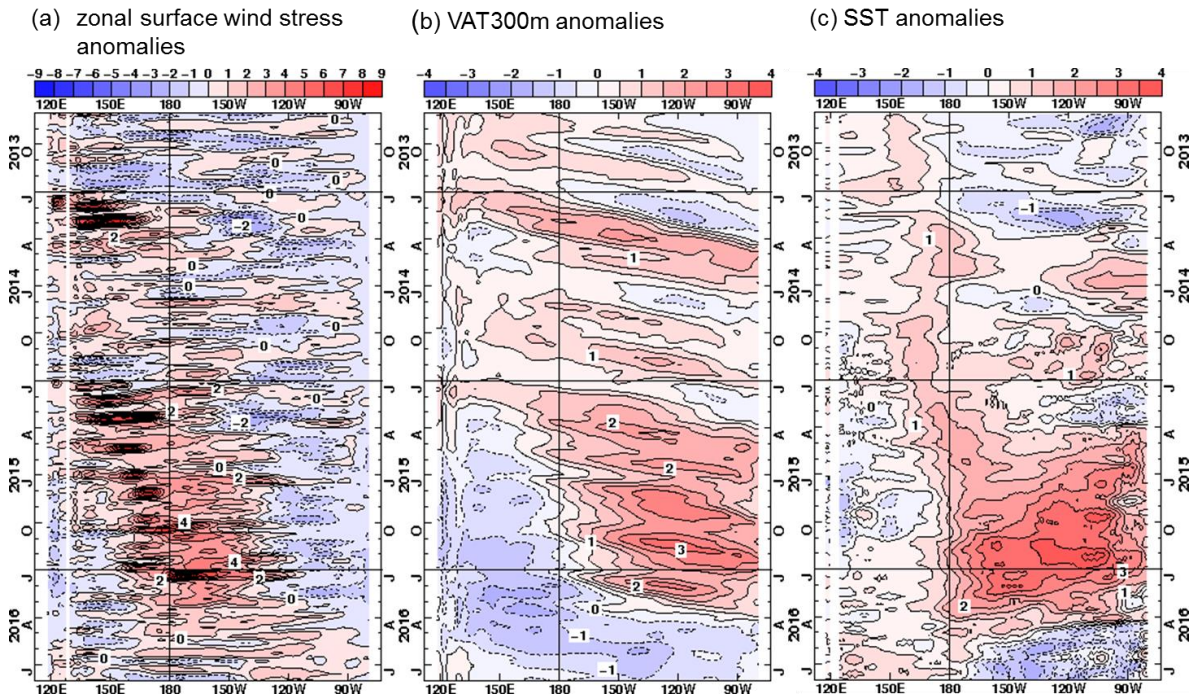

Figure 4 Time-longitude distributions along the equator in the Pacific Ocean from August 2013 to July 2016.
(a) Zonal surface wind stress anomalies ($0.01N/m^2$). Positive values indicate westerly anomalies. (b) Vertically averaged temperature anomalies over the top 300m layer (VAT300m, °C). (c) SST anomalies (°C). The base period for the normal is 1981–2010.

Figure 5a shows SST anomalies for November 2015 during the mature phase of the 2014–16 event. Large positive SST anomalies of up to 3.5°C were observed in central and eastern parts of the equatorial Pacific. The subsurface temperature anomalies along the equatorial Pacific shown in Figure 5b exhibit large zonal contrast, and exceed 7°C around 100°W. For comparison, Figure 6a presents SST anomalies for November 1997 during the mature phase of the 1997–98 El Niño event (one of the strongest since 1949). As in 2015, large positive SST anomalies in the central and eastern equatorial Pacific are observed. However, the center of the anomalies was located farther east in 1997 than in 2015. SST anomalies in the central part of the equatorial Pacific were higher in 2015 than in 1997, while those in the eastern part were lower in 2015 (Figure 7a). Subsurface temperature anomalies in the eastern part of the equatorial Pacific in 1997 (Figure 6b) exceeded 10°C, which is significantly higher than the corresponding figure for 2015 (Figure 5b).

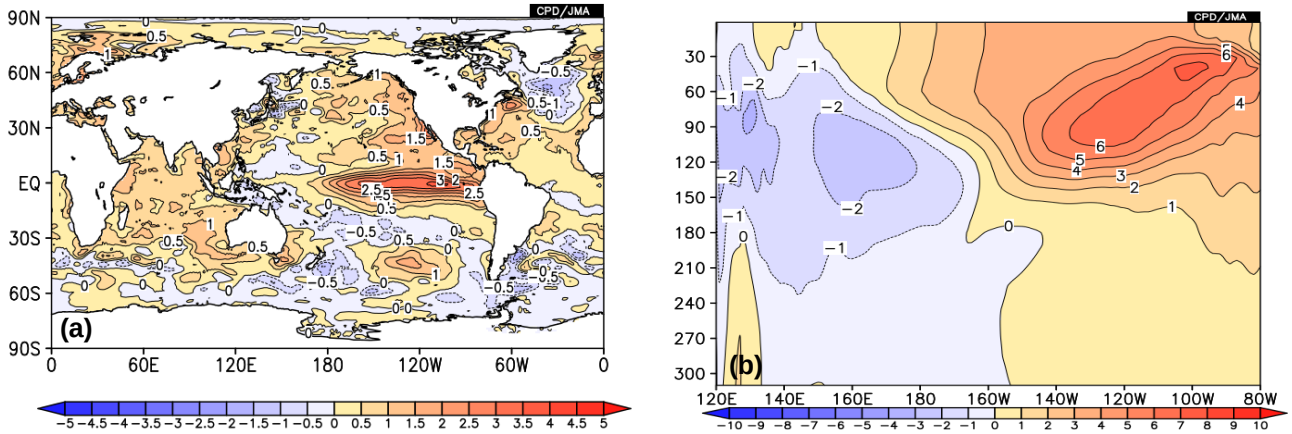

Figure 5 Anomalies of (a) SST and (b) upper ocean temperature along the equatorial Pacific in November 2015. Contour intervals are 0.5°C for (a) and 1°C for (b). The base period for the normal is 1981–2010.

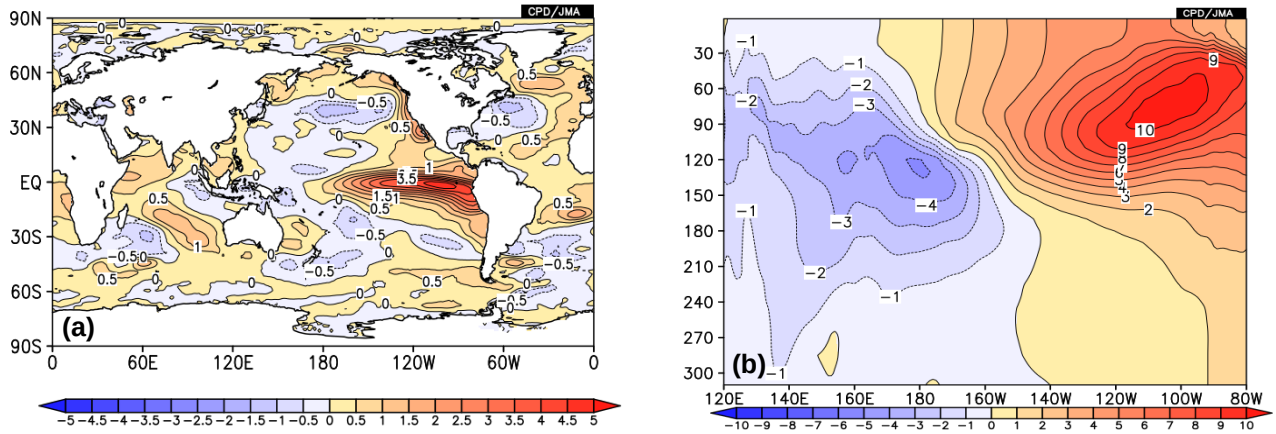

Figure 6 Same as Figure 5 but for November 1997.

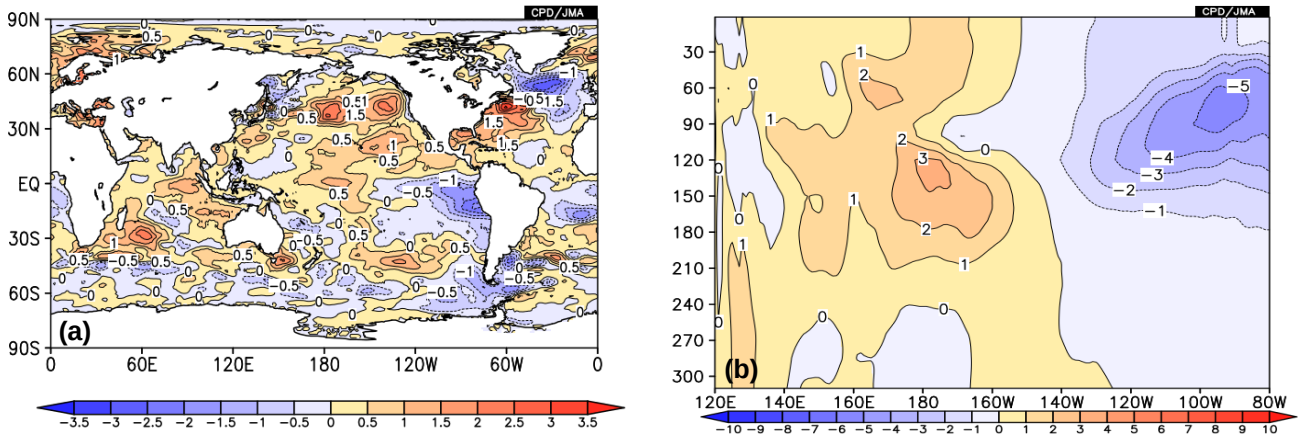

Figure 7 Same as Figure 5 but for anomalies in November 2015 relative to those in November 1997.

3. Climatic impacts of the 2014–16 El Niño event

The annual anomaly of the global average surface temperature in 2015 was +0.42°C above the 1981–2010 average, and was the highest since 1891. The global average surface temperature is affected by natural climate variability on interannual to interdecadal time scales in addition to global warming caused by increased concentrations of greenhouse gases such as CO_2. As the anomaly of the global average surface temperature follows the NINO.3 SST anomaly with a time lag of several months, the record temperatures of 2015 may have been influenced by the El Niño event that began in boreal summer 2014 and developed from boreal spring 2015.

El Niño can also be considered to have affected the Asia-Pacific climate from boreal summer 2015 to boreal winter 2015/2016, bringing high temperatures at low latitudes and low precipitation amounts in and around Indonesia. India and Pakistan experienced heatwaves in May and June 2015, respectively. The six-month mean temperature for July – December 2015 at Hyderabad in southern India was 27.4°C (2.2°C higher than the normal). The total precipitation amount for September – November 2015 at Banjarmasin on Borneo Island in Indonesia was 113 mm (19% of the normal). These figures were consistent with typical anomaly patterns observed in past El Niño events (Figure 8).

Below-normal temperatures and above-normal precipitation amounts were observed in western Japan during boreal summer 2015, while above-normal temperatures and precipitation amounts were observed in Okinawa/Amami and in western/eastern Japan during boreal winter 2015/2016. These characteristics are likely to have been related to atmospheric circulation anomalies, which were mostly consistent with those observed in past El Niño years.

(Tamaki Yasuda and Kenji Kamiguchi, Climate Prediction Division)

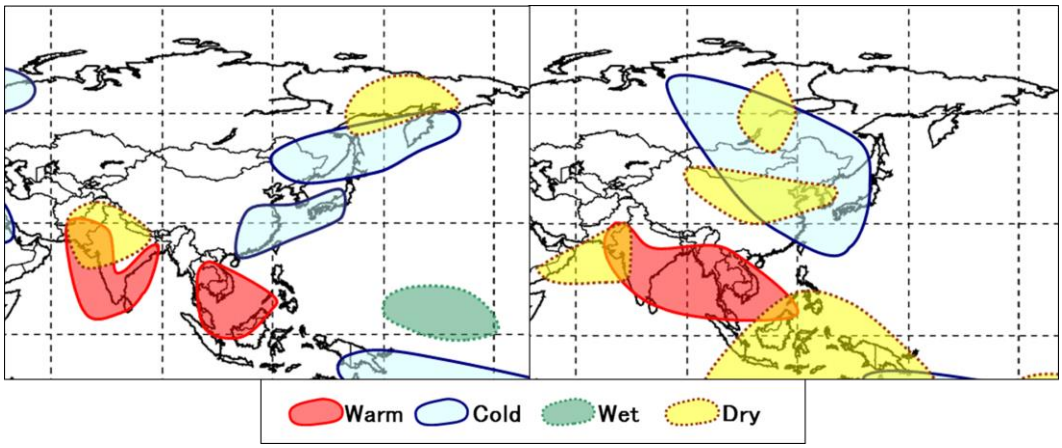

Figure 8 The schematic charts of typical anomaly patterns of surface temperature and precipitation for boreal summer (left) and autumn (right) in past El Niño events.

Sea Ice in the Sea of Okhotsk in the 2015/2016 Winter Season

The maximum sea ice extent in the Sea of Okhotsk for winter 2015/2016 was similar to the normal.

The sea ice extent in the Sea of Okhotsk for winter 2015/2016 was below or near the normal (Figure 9). The seasonal maximum of 1.165 x 10^6 km^2 was reached on 29 February (Figures 9 and 10), and was similar to the normal of 1.169 x 10^6 km^2 (based on the 30-year average from 1980/1981 to 2009/2010). Figure 11 shows the overall trend of maximum sea ice extent from 1971 to 2016. Although values for the Sea of Okhotsk show large interannual variations, there is a long-term downward trend of 0.067 [0.033 – 0.101] x 10^6 km^2 per decade (the numbers in square brackets indicate the two-sided 95% confidence interval), which equates to a loss of 4.3 [2.1 – 6.4]% per decade.

(Ayako Takeuchi, Office of Marine Prediction)

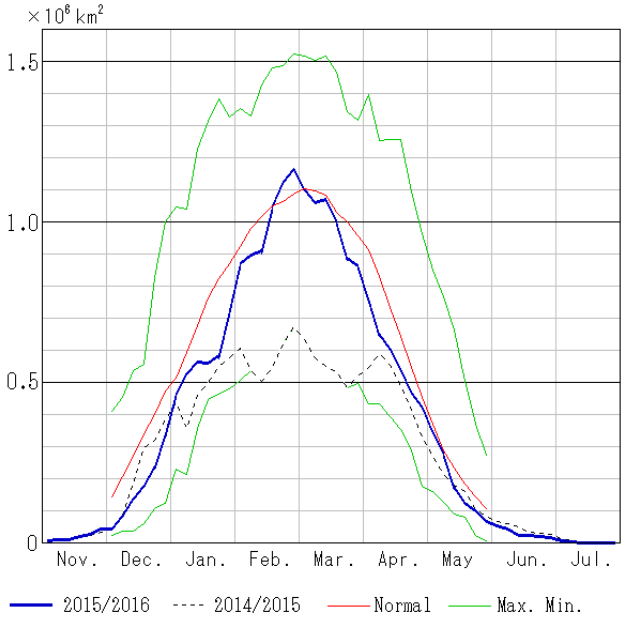

Figure 9 Seasonal variation of sea ice extent at five-day intervals in the Sea of Okhotsk from November 2015 to July 2016.
The normal is the 30-year average from 1980/1981 to 2009/2010).

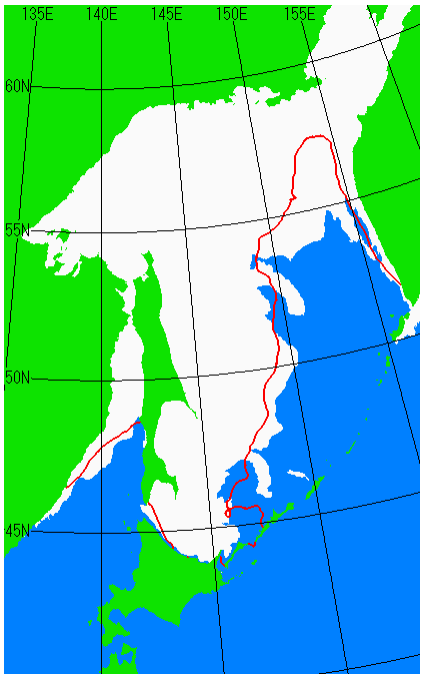

Figure 10 Sea ice situation on 29 February 2016.
The white area shows the observed sea ice extent, and the red line indicates the extent of normal coverage (the 30-year average from 1980/1981 to 2009/2010).

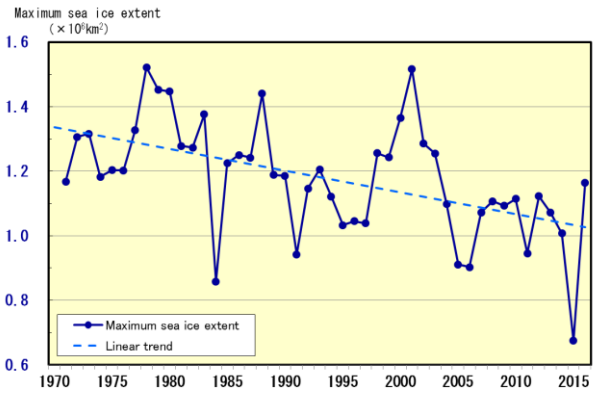

Figure 11 Interannual variation of maximum sea ice extent in the Sea of Okhotsk from 1971 to 2016.
Maximum sea ice extent: the greatest amount of sea ice extent observed during the year

Summary of Kosa (Aeolian dust) Events over Japan in 2016

Characteristics of Kosa events in 2016

Kosa (Aeolian dust) is a meteorological phenomenon in which fine dust is blown up to an altitude of several thousand meters by cyclonic or other wind systems from deserts or cropland in semi-arid areas of the Asian continent, and is transported over long distance by westerly winds, resulting in haze or dustfall in downstream areas. It is often observed between March and May in Japan and makes the sky yellow and hazy. Heavy Kosa can affect transportation by obstructing visibility.

In Japan, 59 JMA meteorological stations (as of 1 August 2016) perform Kosa monitoring based on visibility. From January to June 2016, the number of days on which Kosa was observed at any of these stations (referred to here simply as "the number of Kosa days") was 11, which was approximately half the 1981 – 2010 normal of 23.1. The number of Kosa days in April corresponded to the normal, but was lower in other months (Figure 12, top).

The total number of stations observing Kosa (referred to here simply as "the total number of Kosa stations") over the same period was 96, which was also around half the normal of 208.1. The monthly total number of Kosa stations was lower than the normal from January to June (Figure 12, bottom).

Significant Kosa event in late April

Kosa was extensively observed at stations in Japan from 23 to 26 April 2016 (Figure 13).

Due to a large dust storm in an area of the Gobi Desert around 21 April, massive volumes of dust were blown up into the atmosphere. The surface weather charts in Figure 14 indicate that a low-pressure system moving eastward at 50 degrees north latitude carried dust over to Japan.

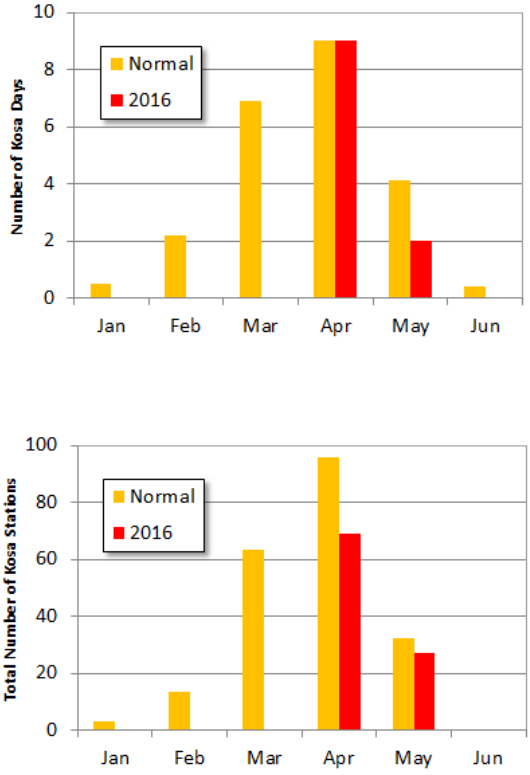

Figure 12 Monthly number of days when meteorological stations in Japan observed Kosa (top), and the monthly total number of stations observing Kosa (bottom) from January to June 2016

The red and yellow bars show the values for 2016 and the 1981 – 2010 normal, respectively.

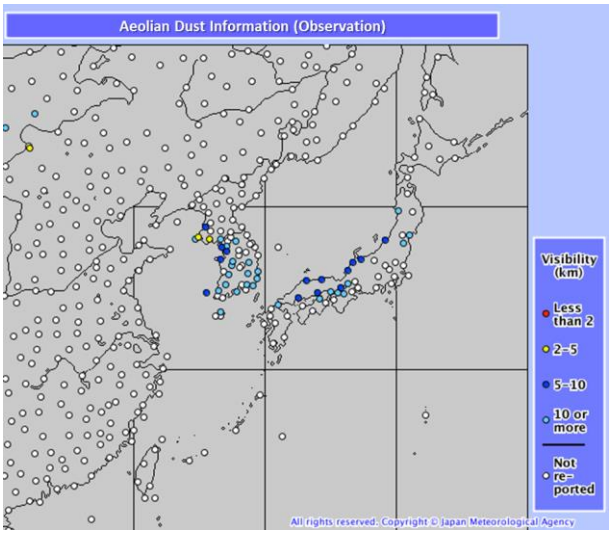

Figure 13 Meteorological stations observing Kosa and minimum visibility on 24 April

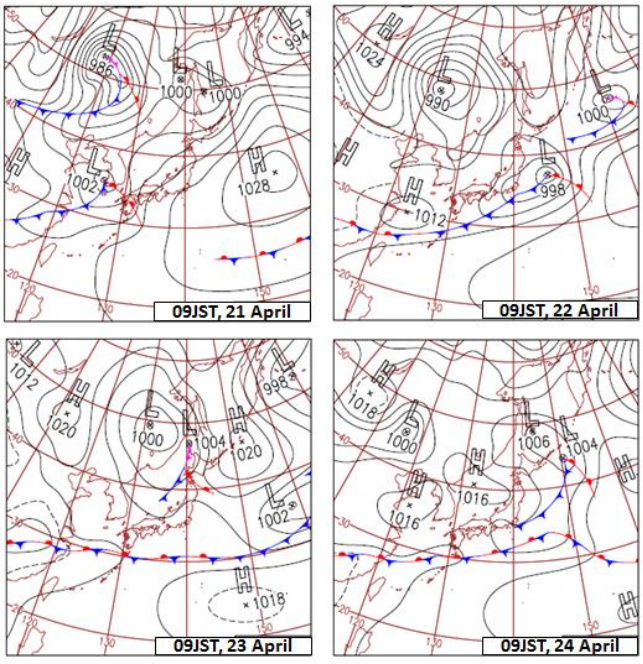

Figure 14 Surface weather analysis chart at 09 JST (00 UTC) on 21, 22, 23, and 24 April

Based on results from JMA's Kosa prediction model, the Kosa was expected to prevail over western Japan on 23 April (Figure 15).

Dust RGB* images created since 2015 using data from a new sensor called the Advanced Himawari Imager (AHI) on board Himawari-8 showed that Kosa particles were blown up by the Gobi Desert storm and carried over to Japan by westerly winds (Figure 16).

In consideration of the forecast results as well as satellite imagery and surface observation reports from meteorological stations, JMA released information on the Kosa event to the public on 23 April in order to call attention to potential traffic hazards relating to visibility degradation.

(Toshiyuki Kitajima and Toshinori Aoyagi, Atmospheric Environment Division)

* Dust RGB is a satellite product synthesized from three infrared bands (B11 (8.6 μm), B13 (10.4 μm) and B15 (12.4 μm)) of Japan's new Himawari-8 geostationary satellite. In RGB images created with the assignment of [B15 – B13] (i.e., the differential of B15 and B13) to red, [B13 – B11] to blue and B13 to green, Kosa is highlighted in pink or magenta. This product is very useful for Kosa monitoring based on the detection of heavy dust areas over the Asian continent.

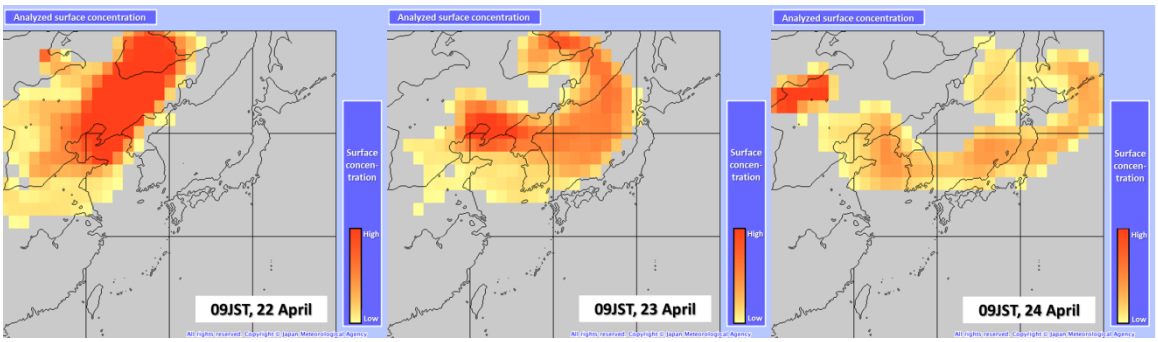

Figure 15 Forecasts of surface dust concentration by JMA's Kosa prediction model at 09 JST (00 UTC) on 22, 23, and 24 April (initial time: 21 JST (12 UTC) on 21 April)

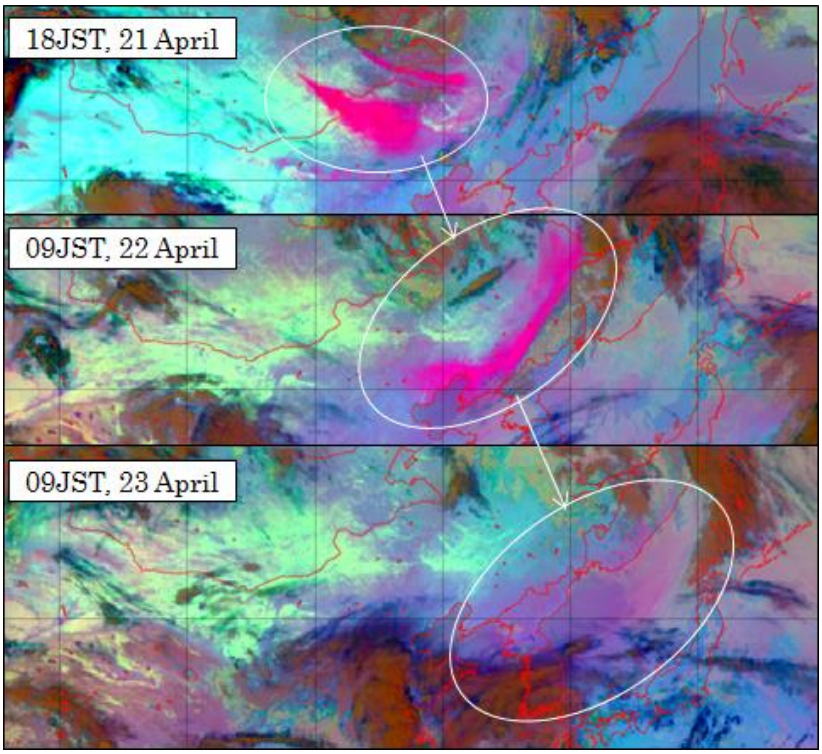

Figure 16 Dust RGB images from Himawari-8 taken at 18 JST (09 UTC) on 21 April, and at 09 JST (00 UTC) on 22, and 23 April. Kosa area appears in pink (magenta).

TCC Experts Visit Cambodia

As part of its support for the capacity-building activities, TCC held annual training seminars on one-month forecasting in 2015 (see TCC News No.42 and TCC website for details of the seminar). The Center also dispatches experts to NMHSs in Southeast Asia and elsewhere for seminar follow-up activities.

From 2 to 4 August 2016, TCC experts paid a visit to Cambodia's Department of Meteorology and held a follow-up seminar on the generation of one-month forecasts using the statistical downscaling technique and on the basic operation of TCC's Interactive Tool for Analysis of the Climate System (iTacs).

The TCC visitors outlined the formulation of statistical guidance for temperature and precipitation with on-site observation data, JMA's one-month re-forecast (hindcast) and operational forecast data. Seminar attendees produced one-month forecasts for regional districts in Cambodia using JMA's guidance tool and iTacs, and made presentations on their achievements on the final day. An introductory presentation on iTacs also provided a good opportunity for the attendees to formulate physical interpretations of the figures created and to acquaint themselves with the operation of the application.

The visit provided outstanding opportunities for the attendees to deepen their understandings of one-month forecasting and to discuss future collaborative work with TCC. TCC will continue to arrange expert visits to NMHSs in the Asia-Pacific region and elsewhere as necessary to assist with operational climate services.

(Masayuki Hirai and Kazuto Takemura, Tokyo Climate Center)

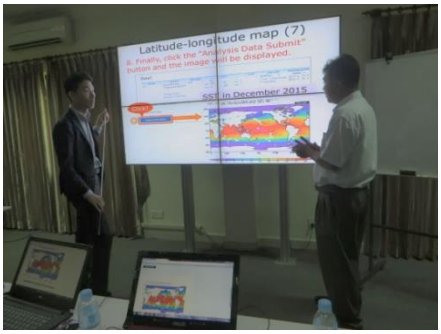

Any comments or inquiry on this newsletter and/or the TCC website would be much appreciated. Please e-mail to tcc@met.kishou.go.jp.

(Editors: Kiyotoshi Takahashi, Atsushi Goto and Yasushi Mochizuki)

Tokyo Climate Center (TCC), Japan Meteorological Agency
Address: 1-3-4 Otemachi, Chiyoda-ku, Tokyo 100-8122, Japan
TCC Website: http://ds.data.jma.go.jp/tcc/tcc/index.html